On the Design of Energy Preserving and Decaying Schemes for Flexible, Nonlinear Multi-Body Systems *

O.A. Bauchau
Georgia Institute of Technology,
School of Aerospace Engineering.
Atlanta, Georgia, 30332, USA.
and
Carlo L. Bottasso
Politecnico di Milano
School of Aerospace Engineering

Abstract

Energy preserving schemes achieve unconditional stability for nonlinear systems by establishing discrete energy preservation statements. Several schemes have been presented by various authors within drastically different frameworks: finite difference schemes based on a mid-point approximation, Galerkin and time discontinuous Galerkin approximations of the equations of motion written in the symmetric hyperbolic form, finite elements in time, and 2-stage FSAL Runge-Kutta methods. Furthermore, different types of parameterization of finite rotations were used in the various formulations. This paper presents a unified, finite difference framework which readily allows comparing the various schemes and their respective properties. Numerical examples are presented and show that the predictions of two of these schemes are in very close agreement with each other.

1 Introduction

This paper is concerned with the dynamic analysis of flexible, nonlinear multi-body systems, *i.e.* a collection of bodies in arbitrary motion with respect to each other while each body is undergoing large displacements and rotations with respect to a body attached frame of reference. The focus is on problems where strain within each elastic body remains small.

The elastic bodies are modeled using the finite element method. The location of each node is represented by its Cartesian coordinates in an inertial frame, and the orientation of

* *Computer Methods in Applied Mechanics and Engineering*, **169**, 1999, pp 61-79.

a local frame at each node is represented by a finite rotation tensor expressed in the same inertial frame. The kinematic constraints among the various bodies are enforced via the Lagrange multiplier technique. Although this approach does not involve the minimum set of coordinates, it allows a modular development of finite elements for the enforcement of the kinematic constraints.

The equations of motion resulting from the modeling of multi-body systems with the above methodology present distinguishing features: they are stiff, nonlinear, differential-algebraic equations. The stiffness of the system stems not only from the presence of high frequencies in the elastic members, but also from the infinite frequencies associated with the kinematic constraints. Indeed, no mass is associated with the Lagrange multipliers giving rise to algebraic equations coupled to the other equations of the system which are differential in nature.

The time integration of the resulting equations of motion gives rise to a number of problems such as numerical instabilities and high frequency oscillations of a purely numerical origin. A thorough review of time integration schemes used in structural dynamics is found in [1]. The Newmark scheme [2] is widely used to integrate the equations of motion resulting from finite element discretizations. Cardona and Géradin [3] have shown that this scheme presents a weak instability when applied to constrained multi-body systems. The culprit is the presence of algebraic equations which are equivalent to infinite frequencies.

The Hilber-Hughes-Taylor (HHT) [4] scheme was introduced to eliminate the high frequency oscillations of a purely numerical origin resulting from the use of the Newmark scheme for large finite element problems. Indeed, larger and larger finite element models present higher and higher frequencies which in turns generate high frequency oscillations. The HHT scheme alleviates this problem by introducing high frequency numerical dissipation. Cardona and Geradin [3] have shown that the use of the HHT scheme in constrained multi-body problems can yield satisfactory system response. Numerical oscillations are observed in the response of accelerations, Lagrange multipliers, and velocities, though to a lesser extent. However, these high frequency oscillations rapidly damp out. As the complexity of the constrained multi-body system increases, an increasing amount of numerical dissipation is required to avoid numerical instabilities and high frequency oscillations.

More recently, energy preserving and decaying schemes have been presented by a number of authors for various structural dynamics problems. Although all schemes share the same goal of achieving unconditional stability for nonlinear problems by establishing discrete energy preservation or decay properties of the algorithm, they have been introduced within drastically different frameworks. Simo and his co-workers presented energy preserving schemes for rigid body dynamics [5], elasto-dynamics [6], and beams [7]. These schemes were presented as second order accurate, finite difference schemes based on a mid-point approximation. Finite rotations were parameterized with the rotation vector, then using Cayley's algebraic form of finite rotations. Bauchau and his co-workers presented both energy preserving and decaying schemes for beams [8], elasto-dynamics [9], and multi-body systems [10]. These schemes originate from Galerkin and time discontinuous Galerkin approximations of the equations of motion written in the symmetric hyperbolic form. Finite rotations were parameterized using the conformal rotation parameters, then Rodrigues parameters. Finally, Bottasso and Borri proposed both energy preserving and decaying schemes for beams [11, 12] and multi-body systems [13, 14]. Their schemes were cast within the framework of finite

elements in time at first, then as 2-stage FSAL Runge-Kutta methods. The rotation vector was used to represent finite rotations.

The goal of this paper is to assess the merits of these seemingly different schemes. To that effect, the various families of schemes will be presented within a unified, finite difference framework, starting from the equations of motion written in the moving or fixed pole formulations. It will be shown that for all cases, the discrete energy preservation property requires the average velocity vector to be the eigenvector associated with the unit eigenvalue of an eigenproblem involving discretized operators. The schemes will be presented in terms of a novel representation of finite rotations, called the generic rotation parameters, to emphasize the fact that most schemes can be used with any valid parameterization of finite rotations. In addition to discrete energy preservation, some schemes are also momentum preserving. Finally, some schemes are invariant with respect to the choice of reference point; for example, in the case of the beam, they are invariant with respect to the placement of the beam reference line.

This paper is organized in the following manner. Kinematic notations and conventions are described in section 2, and section 3 introduces the generic finite rotation parameters used throughout this work. Section 4 develops the equations of motion for beams undergoing arbitrarily large displacements and rotations but small strains, in both moving and fixed poles forms. Sections 5 and 6 then present three different energy preserving schemes based on the moving and fixed pole formulations, respectively. The properties of these schemes are compared in section 7 and the extension of energy preserving to energy decaying algorithms is discussed in section 8. Section 9 briefly addresses the analysis of constrained mechanical systems, while retaining the conservation laws that guarantee nonlinear unconditional stability. Finally, numerical examples are presented in section 10.

2 Kinematic notations and conventions

The kinematic description of bodies and joints in their reference and actual configurations will make use of three orthogonal triads. First, an inertial triad is used as a global reference for the system; it is denoted $\mathcal{S}_I$ with unit vectors $\vec{\imath}_1$, $\vec{\imath}_2$, and $\vec{\imath}_3$ and origin O. A second triad $\mathcal{S}_0$, with unit vectors $\vec{e}_{01}$, $\vec{e}_{02}$, and $\vec{e}_{03}$ and origin P_0 is attached to the body and defines its orientation in the reference configuration. Finally, a third triad $\mathcal{S}^*$ with unit vectors $\vec{e}_1$, $\vec{e}_2$, and $\vec{e}_3$ and origin P defines the orientation of the body in its actual configuration.

Let $\vec{u}_0$ and $\vec{u}$ be the displacement vectors from $\mathcal{S}_I$ to $\mathcal{S}_0$, and $\mathcal{S}_0$ to $\mathcal{S}^*$, respectively, and $\mathbf{R}_0$ and $\mathbf{R}$ the rotation tensors from $\mathcal{S}_I$ to $\mathcal{S}_0$, and $\mathcal{S}_0$ to $\mathcal{S}^*$, respectively. In this work, all vector and tensor components are measured in either $\mathcal{S}_I$ or $\mathcal{S}^*$. For instance, the components of vector $\vec{u}$ measured in $\mathcal{S}_I$ and $\mathcal{S}^*$ will be denoted $\underline{u}$ and $\underline{u}^*$, respectively. Similarly, the components of tensor $\mathbf{R}$ measured in $\mathcal{S}_I$ and $\mathcal{S}^*$ will be denoted R and R^*, respectively. The components $\underline{u}$ and $\underline{u}^*$ are related by the expression

$$\underline{u}^* = \alpha^T \, \underline{u}, \tag{1}$$

where

$$\alpha = R R_0. \tag{2}$$

The skew-symmetric matrix formed with the components $\underline{u}$ will be denoted $\widetilde{u}$.

For brevity sake, a compact notation will be used to deal with the components of the linear and angular vectors simultaneously. For instance,

$$\underline{v} = \begin{bmatrix} \hat{\underline{v}} \\ \check{\underline{v}} \end{bmatrix} \tag{3}$$

defines the six components of the velocity vector consisting of the three components of linear and angular velocities denoted $\hat{\underline{v}}$ and $\check{\underline{v}}$, respectively. The following 6×6 operators are introduced

$$A = \begin{bmatrix} \alpha & 0 \\ 0 & \alpha \end{bmatrix}, \quad U[\bullet] = \begin{bmatrix} 0 & 0 \\ [\widetilde{\bullet}] & 0 \end{bmatrix}, \quad V[\bullet] = \begin{bmatrix} [\widetilde{\bullet}] & 0 \\ 0 & 0 \end{bmatrix}. \tag{4}$$

3 The generic rotation parameters

Although energy preserving schemes have been presented in the literature with specific rotation parameters, most schemes presented in this work will be expressed in term of a novel definition of rotation parameters, named *generic finite rotation parameters*, and defined as

$$\underline{p} = p[\phi]\ \underline{a}, \tag{5}$$

where $\underline{a}$ is the unit vector about which a finite rotation of magnitude ϕ is taking place. The norm p of the generic parameters is assumed to be a sole function of ϕ, with $f = \mathrm{d}p[\phi]/\mathrm{d}\phi$ denoting its derivative with respect to ϕ. The following condition will be met by $p[\phi]$

$$\lim_{\phi \to 0}\ p[\phi] = \phi, \tag{6}$$

implying that for small rotation, the generic parameters are identical to the infinitesimal rotation vector. Note that definition (5) encompasses several commonly used parameterizations, as shown in Table 1 which lists various choices of $p[\phi]$. Details about these various parameterizations can be found in numerous textbooks such as [15, 16], or reports [17].

Table 1: Particular choices of $p[\phi]$ for the generic parameters.

Parameterization	$p[\phi]$	$f[\phi]$
Rotation vector	ϕ	1
Linear parameters	$\sin[\phi]$	$\cos[\phi]$
Reduced Euler parameters	$2\sin[\phi/2]$	$\cos[\phi/2]$
Rodrigues parameters	$2\tan[\phi/2]$	$\cos^{-2}[\phi/2]$
Conformal rotation parameters	$4\tan[\phi/4]$	$\cos^{-2}[\phi/4]$

The rotation tensor can be expressed in terms of the generic parameters as

$$R[\underline{p}] = I + \frac{\sin\phi}{p}\ \widetilde{p} + \frac{1-\cos\phi}{p^2}\ \widetilde{p}\widetilde{p}. \tag{7}$$

The angular velocity vector $\check{\underline{v}}$ can be expressed as

$$\check{\underline{v}} = H[\underline{p}]\ \dot{\underline{p}}, \tag{8}$$

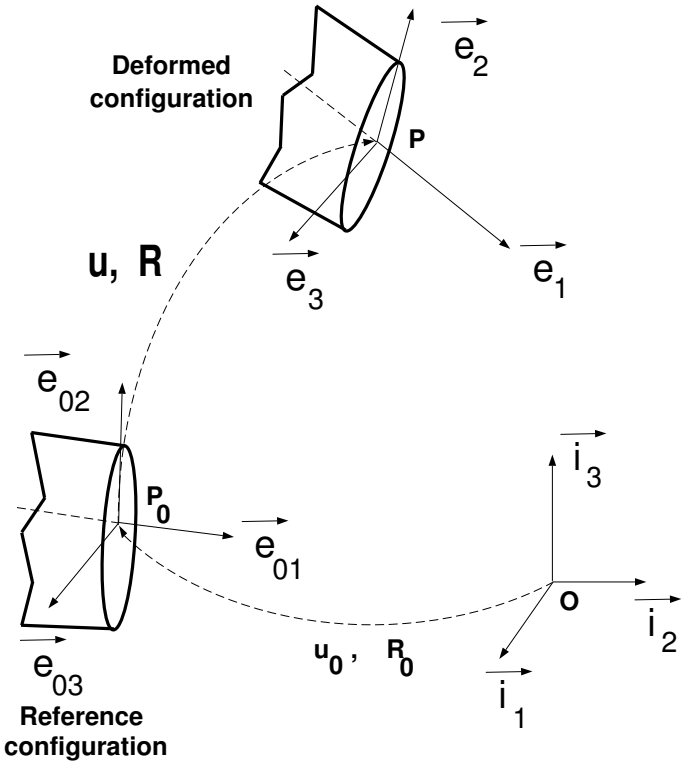

Figure 1: Beam in the reference and actual configurations.

where the operator H is found to be

$$H[\underline{p}] = \frac{I}{f} + \frac{1-\cos\phi}{p^2}\,\widetilde{p} + \frac{1}{p^2}\left(\frac{1}{f} - \frac{\sin\phi}{p}\right)\,\widetilde{p}\widetilde{p}. \tag{9}$$

The following two decompositions of the rotation tensor will be extensively used in this work

$$R = HH^{-T} = H^{-T}H, \tag{10}$$

and

$$R = \left(I + \epsilon\frac{\tilde{p}}{2}\right)\left(I + \epsilon\frac{\tilde{p}}{2}\right)^{-T} = \left(I + \epsilon\frac{\tilde{p}}{2}\right)^{-T}\left(I + \epsilon\frac{\tilde{p}}{2}\right), \tag{11}$$

where

$$\epsilon = \frac{2\tan[\phi/2]}{p}. \tag{12}$$

4 Formulation of beam equations

In this section, the equations of motions governing three-dimensional elastic beams are developed. Flexible joints, *i.e.* elements that model generic elastic couplings between two bodies, can be readily developed starting from the beam schemes, as discussed in [18].

Beams can be defined as elastic bodies whose volume is that spanned by a cross-section translating along a smooth reference line. The cross-section lies in the plane defined by vectors $\vec{e}_{02}$, $\vec{e}_{03}$ and $\vec{e}_2$, $\vec{e}_3$ in the reference and actual configurations, respectively, as depicted in fig. 1. The kinetic and strain energies of the beam are

$$\mathcal{K} = \frac{1}{2}\int_0^L \underline{v}^{*T}\underline{p}^* \, \mathrm{d}x_1, \quad \mathcal{V} = \frac{1}{2}\int_0^L \underline{e}^{*T}\underline{f}^* \, \mathrm{d}x_1, \tag{13}$$

respectively. L is the length of the beam; x_1 the curvilinear coordinate along the reference line; $\underline{p}^* = M^* \, \underline{v}^*$ and $\underline{f}^* = K^* \, \underline{e}^*$ are the sectional momenta and elastic forces, respectively. $\underline{v}^*$ and $\underline{e}^*$ are the components of the sectional velocity and strain vectors, respectively. M^* is the 6×6 inertial matrix, allowing the modeling of rotary inertia effects and the offset of the sectional mass center with respect to the reference line. Similarly, the 6×6 stiffness matrix K^* is fully populated, allowing the modeling of shearing deformation effect, the offset of tension center and shear center with respect to the reference line, and all elastic couplings that might arise from the use of tailored composite materials. The velocity-displacement and strain-displacement relationships are

$$\underline{v} = \begin{bmatrix} \underline{\hat{v}} \\ \underline{\check{v}} \end{bmatrix} = \begin{bmatrix} \underline{\dot{u}} \\ H[\underline{p}] \, \underline{\dot{p}} \end{bmatrix}, \tag{14}$$

$$\underline{e} = \begin{bmatrix} \underline{\hat{e}} \\ \underline{\check{e}} \end{bmatrix} = \begin{bmatrix} (\underline{u}_0' + \underline{u}') - R \, \underline{u}_0' \\ \underline{k} - R \, \underline{k}_0 \end{bmatrix}, \tag{15}$$

respectively, where $[\bullet]^{\cdot}$ and $[\bullet]'$ denote derivatives with respect to time and x_1, respectively; $\underline{\check{v}}$ are the components of the sectional angular velocity vector, with $\widetilde{\check{v}} = \dot{\alpha}\alpha^T$; $\underline{k}$ are the components of the sectional curvature vector, with $\widetilde{k} = \alpha'\alpha^T$, and in the reference configuration $\widetilde{k}_0 = R_0' R_0^T$.

These relationships are geometrically exact, *i.e.* are valid for arbitrarily large displacements and rotations, although the strains are assumed to remain small. Virtual variations in sectional velocities and strains are

$$\delta\underline{v}^{*T} = \left(\underline{\delta\dot{d}}^T - \underline{\delta d}^T \, U[\dot{u}]\right) A, \tag{16}$$

$$\delta\underline{e}^{*T} = \left(\underline{\delta d}'^T - \underline{\delta d}^T \, U[u_0' + u']\right) A, \tag{17}$$

where $\underline{\delta d}^T = (\underline{\delta u}^T, \ \underline{\delta\psi}^T)$ are the virtual displacements and rotations. The virtual rotations are defined as $\widetilde{\delta\psi} = \delta R \, R^T$.

The equations of motion of the beam will be derived from Hamilton's principle

$$\int_{t_i}^{t_f}\int_0^L \left(\delta\underline{v}^{*T}\underline{p}^* - \delta\underline{e}^{*T}\underline{f}^* + \delta\mathcal{W}^a\right) \mathrm{d}x_1 \, \mathrm{d}t = 0, \tag{18}$$

where $\delta\mathcal{W}^a$ is the virtual work done by the externally applied forces $\underline{q}$. The equations of motion of the beam are found by introducing eqs. (16) and (17), and using the strain and velocity expressions, eqs. (14,15), to find

$$\left(A \, \underline{p}^*\right)^{\cdot} + U[\dot{u}] \, A\underline{p}^* - \left(A\underline{f}^*\right)' - U[u_0' + u'] \, A\underline{f}^* = \underline{q}. \tag{19}$$

In this work, an alternate form of the equations of motion, called *fixed pole* form [12] is also considered. In this approach, the sectional forces $\underline{f}_{(O)}$ computed with respect to the inertial point O are evaluated

$$\underline{f}_{(O)} = \begin{bmatrix} \hat{\underline{f}} \\ \check{\underline{f}} + (\widetilde{u}_0 + \widetilde{u})\hat{\underline{f}} \end{bmatrix} = C^{-T}\underline{f}^*. \tag{20}$$

The sectional force is unaltered, while the sectional moment is affected by the term $(\widetilde{u}_0+\widetilde{u})\hat{\underline{f}}$. In a similar manner, the momenta computed with respect to the origin become

$$\underline{p}_{(O)} = C^{-T}\underline{p}^*. \tag{21}$$

$\mathbf{C}$ is termed the *configuration tensor*, with components C,

$$C = TA; \quad T = \begin{bmatrix} I & (\widetilde{u}_0 + \widetilde{u}) \\ 0 & I \end{bmatrix}. \tag{22}$$

A is the *convection operator*, and transforms vector components from the $\mathcal{S}^*$ to the $\mathcal{S}_I$ frame. T is termed the *transport operator*. More details about the properties of the configuration tensor are explored in [12].

The kinetic and strain energies (13) are frame invariant and can, therefore, be written as

$$\mathcal{K} = \frac{1}{2}\int_0^L \underline{v}_{(O)}^T\, \underline{p}_{(O)}\, \mathrm{d}x_1, \quad \mathcal{V} = \frac{1}{2}\int_0^L \underline{e}_{(O)}^T\, \underline{f}_{(O)}\, \mathrm{d}x_1. \tag{23}$$

The energetically conjugated *fixed pole velocities*, and *fixed pole strains* are given by

$$\underline{v}_{(O)} = C\,\underline{v}^*; \quad \underline{e}_{(O)} = C\,\underline{e}^*, \tag{24}$$

respectively. Note that $\underline{v}_{(O)}$ writes

$$\underline{v}_{(O)} = \begin{bmatrix} \hat{\underline{v}} + (\widetilde{u}_0 + \widetilde{u})\,\check{\underline{v}} \\ \check{\underline{v}} \end{bmatrix}. \tag{25}$$

The fixed pole angular velocity is unaffected by the transport to the fixed pole, while the fixed pole linear velocity becomes $\hat{\underline{v}}_{(O)} = \hat{\underline{v}} + (\widetilde{u}_0 + \widetilde{u})\,\check{\underline{v}}$.

The fixed pole velocity can be interpreted as the *co-rotational derivative* of the position vector, *i.e.* the time derivative of the position vector as viewed by an observer attached to $\mathcal{S}^*$. It can also be interpreted as the instantaneous velocity of the point of a rigid body attached to $\mathcal{S}^*$ which location coincides with that of the inertial reference point O. This latter interpretation has suggested the name of *fixed pole velocity*.

The *fixed pole* form of the equation of motion is now readily obtained from Hamilton's principle, together with (23)

$$\dot{\underline{p}}_{(O)} - \underline{f}'_{(O)} = \underline{q}_{(O)}. \tag{26}$$

It is interesting to observe that, while the standard linear velocity $\hat{\underline{v}}$ clearly depends on the choice of the reference point, the fixed pole velocity $\hat{\underline{v}}_{(O)}$ is invariant, *i.e.* it is identical for

all points of the cross-section. Since $\underline{\check{v}}$ is also unique for any cross section, $\underline{v}_{(O)}$ is a unique property of the frames associated with each cross section. This means that schemes based on discretizations of eq. (19) will yield results that are affected by the choice made for the placement of the reference line, while schemes based on discretizations of eq. (26) will be invariant.

The preservation of the total mechanical energy of the system can be verified by computing the work done by the inertial and elastic forces

$$\int_0^L \underline{v}_{(O)}^T \, \underline{\dot{p}}_{(O)} \, \mathrm{d}x_1 = \dot{\mathcal{K}}; \quad \int_0^L \underline{v}_{(O)}^T \, \underline{f}'_{(O)} \, \mathrm{d}x_1 = \dot{\mathcal{V}}. \tag{27}$$

As a result, in the absence of externally applied loads, eqs. (26) imply

$$(\mathcal{K} + \mathcal{V})^{\cdot} = 0, \tag{28}$$

the preservation of the total mechanical energy of the system.

Furthermore, integration of the equations of motion over the length of the beam in the case of pure Neumann boundary conditions, yields

$$\left(\int_0^L \underline{p}_{(O)} \, \mathrm{d}x_1 \right)^{\cdot} = 0. \tag{29}$$

Eq. (29) then implies the conservation of the total fixed pole momentum in the absence of externally applied loads.

5 Energy preserving schemes derived from the moving pole equations

Consider a typical time step from time t_i to time t_f, of size $\Delta t = t_f - t_i$. The subscripts $(.)_f$ and $(.)_i$ will be used to denote the values of the corresponding quantities at times t_f and t_i, respectively. The following discretization of the equations of motion in the moving pole form, eqs. (19), is proposed

$$\frac{A_f M^* \underline{v}_f^* - A_i M^* \underline{v}_i^*}{\Delta t} + U\,[\underline{\hat{v}}_m] \, \frac{A_m^{v_f} M^* \underline{v}_f^* + A_m^{v_i} M^* \underline{v}_i^*}{2} \\ - (A_m^e K^* \underline{e}_m^*)' - \epsilon \, U\,[\underline{u}_0' + \underline{u}_m'] \, A_m^e K^* \underline{e}_m^* = \underline{q}_m, \tag{30}$$

where $\underline{u}_m = (\underline{u}_f + \underline{u}_i)/2$. The initial and final positions are related by the following update formulas

$$\underline{u}_f = \underline{u}_i + \Delta t \, \underline{\hat{v}}_m, \tag{31}$$

$$\alpha_f = \alpha_i \, R^*[\underline{p}^*], \quad \underline{p}^* = \Delta t \, \underline{\check{v}}_m^*. \tag{32}$$

The subscript $(.)_m$ denotes the mid-point, or average value of a quantity. Hence, $\underline{v}_m$ and $\underline{e}_m$ are the average velocities and strains, respectively. $A_m^{v_f}$, $A_m^{v_i}$, and A_m^e are yet unknown, suitable approximations of the convection operator A. The components of the average velocity in frames $\mathcal{S}_I$ and $\mathcal{S}^*$ are related as follows

$$\underline{v}_m = A_m \, \underline{v}_m^*, \tag{33}$$

where A_m is again a suitable approximation of A, yet to be determined. In section 4 it was shown that the equations of motion imply the conservation of the total mechanical energy. We show in the following that the discrete eqs. (30) imply a discrete energy preservation statement in the absence of externally applied loads, for a suitable choice of the undetermined quantities. To this effect, the work done by the discretized inertial forces $\mathcal{W}^I$ is computed by multiplying eqs. (30) by $\Delta t\ \underline{v}_m^T$ and integrating over the beam to find

$$\begin{aligned}\mathcal{W}^I = \int_0^L \underline{v}_m^T \left(\left(A_f + \frac{\Delta t}{2} U[\hat{\underline{v}}_m] A_m^{v_f} \right) M^* \underline{v}_f^* - \left(A_i - \frac{\Delta t}{2} U[\hat{\underline{v}}_m] A_m^{v_i} \right) M^* \underline{v}_i^* \right) \mathrm{d}x_1 \\ = \int_0^L \underline{v}_m^{*T} \left(\left(A_m^T A_f - \frac{\Delta t}{2} A_m^T V[\check{\underline{v}}_m] A_m^{v_f} \right) M^* \underline{v}_f^* \right. \\ \left. - \left(A_m^T A_i + \frac{\Delta t}{2} A_m^T V[\check{\underline{v}}_m] A_m^{v_i} \right) M^* \underline{v}_i^* \right) \mathrm{d}x_1. \quad (34)\end{aligned}$$

If the approximations A_m, $A_m^{v_f}$ and $A_m^{v_i}$ satisfy the following conditions

$$\left(A_m^T A_f - \frac{\Delta t}{2} A_m^T V[\check{\underline{v}}_m] A_m^{v_f} \right)^T \underline{v}_m^* = \underline{v}_m^*, \quad (35)$$

$$\left(A_m^T A_i + \frac{\Delta t}{2} A_m^T V[\check{\underline{v}}_m] A_m^{v_i} \right)^T \underline{v}_m^* = \underline{v}_m^*, \quad (36)$$

and the average velocity $\underline{v}_m^*$ is simply chosen as the mid-point approximation

$$\underline{v}_m^* = \frac{\underline{v}_f^* + \underline{v}_i^*}{2}, \quad (37)$$

then, eq. (34) implies

$$\mathcal{W}^I = \int_0^L \frac{1}{2} (\underline{v}_f^* + \underline{v}_i^*)^T M^* (\underline{v}_f^* - \underline{v}_i^*) \, \mathrm{d}x_1 = \mathcal{K}_f - \mathcal{K}_i. \quad (38)$$

This establishes that the work done by the inertial forces over one time step is equal to the change in kinetic energy if conditions (35) and (36) are satisfied.

Next, the work done by the elastic forces $\mathcal{W}^e$ is evaluated by multiplying eqs. (30) by $\Delta t\ \underline{v}_m^T$ and integrating over the beam to find

$$\begin{aligned}\frac{\mathcal{W}^e}{\Delta t} = \int_0^L \left(\underline{v}_m^T \left(A_m^e K^* e_m^* \right)' + \underline{v}_m^T U \left[\underline{u}_0' + \underline{u}_m' \right] A_m^e K^* e_m^* \right) \mathrm{d}x_1 \\ = \int_0^L \left(-\underline{v}_m'^T + \underline{v}_m^T \, \epsilon \, U \left[\underline{u}_0' + \underline{u}_m' \right] \right) \, A_m^e K^* e_m^* \, \mathrm{d}x_1. \quad (39)\end{aligned}$$

The boundary term $\underline{v}_m^T A_m^e K^* e_m^* |_0^L$ resulting from the integration by parts vanishes, because either a boundary is unconstrained and the internal forces are zero, or a boundary is constrained and the corresponding velocity components are zero. The updates eqs. (31, 32)

imply the following relations between the strain increments, and the spatial derivative of the average velocity

$$\hat{\underline{e}}_f^* - \hat{\underline{e}}_i^* = \left(\frac{\alpha_f + \alpha_i}{2}\right)^T \Delta t \ \left(\hat{\underline{v}}'_m - \epsilon \ \widetilde{\check{v}}_m(\underline{u}'_0 + \underline{u}'_m)\right), \tag{40}$$

$$\check{\underline{e}}_f^* - \check{\underline{e}}_i^* = \alpha_i^T H^T \Delta t \, \check{\underline{v}}'_m. \tag{41}$$

These relationships can be solved for $\underline{v}'_m$, and the results introduced in eq. (39). A_m^e is selected as

$$A_m^e = \begin{bmatrix} \dfrac{\alpha_f + \alpha_i}{2} & 0 \\ 0 & H\alpha_i \end{bmatrix}. \tag{42}$$

Note that this choice is such that the corresponding terms of $\underline{v}'_m$ cancel out. If the average strains are computed using the mid point rule

$$\underline{e}_m^* = \frac{\underline{e}_f^* + \underline{e}_i^*}{2}, \tag{43}$$

eq. (39) then becomes

$$\mathcal{W}^e = \int_0^L \frac{1}{2}(\underline{e}_f^* + \underline{e}_i^*)^T K^*(\underline{e}_f^* - \underline{e}_i^*) \, \mathrm{d}x_1 = \mathcal{V}_f - \mathcal{V}_i, \tag{44}$$

i.e. the work done by the elastic forces over one time step is equal to the change in strain energy. Combining eqs. (38) and (44), it is now clear that (30) implies

$$\mathcal{K}_f + \mathcal{V}_f = \mathcal{K}_i + \mathcal{V}_i. \tag{45}$$

In summary, discretization (30) imply the discrete total energy preservation statement (45), provided that conditions (35) and (36) are satisfied. Two schemes will now be presented that only differ in the specific choice of A_m, $A_m^{v_f}$ and $A_m^{v_i}$ that will satisfy conditions (35) and (36).

5.1 *Scheme 1*

Scheme 1 is characterized by the following choice of operators

$$A_m = \frac{A_f + A_i}{2}, \quad A_m^{v_f} = \epsilon A_f, \quad A_m^{v_i} = \epsilon A_i, \tag{46}$$

where ϵ is given by eq. (12). This choice satisfies the angular part of condition (35), indeed

$$\alpha_f^T \, \frac{\alpha_f + \alpha_i}{2} \, \check{\underline{v}}_m^* = \frac{R^{*T} + I}{2} \, \check{\underline{v}}_m^* = \check{\underline{v}}_m^*, \tag{47}$$

where we have used the orientation update eq. (32) and the parallelism of the generic parameter vector with the angular velocity implied by $\underline{p}^* = \Delta t \ \check{\underline{v}}_m^*$. Turning now to the linear

part of the same condition, we find

$$\alpha_f^T \frac{\alpha_f + \alpha_i}{2} + \frac{\Delta t}{2} \epsilon \alpha_f^T \widetilde{\breve{v}}_m \frac{\alpha_f + \alpha_i}{2}$$
$$= \frac{1}{2}\left(R^{*T} + I + \frac{\epsilon}{2}\alpha_f^T \widetilde{p} \alpha_f R^{*T} + \frac{\epsilon}{2}\alpha_f^T \widetilde{p} \alpha_f\right)$$
$$= \frac{1}{2}\left(I - \frac{\epsilon}{2}\widetilde{p}^* + I + \frac{\epsilon}{2}\widetilde{p}^*\right) = I, \tag{48}$$

where property (11) of generic rotation parameters was used. Condition (35) is then verified, and condition (36) can be proven in a similar manner.

Note that the choice of parameterization of rotations affects the discrete equations of motion through the parameter ϵ. The coefficient ϵ is simply equal to unity for Rodrigues parameters, see Table 1.

The algorithm proposed by Simo *et al.* in [7] is a special case of the scheme described above. In their work, Simo and co-workers chose the origin P of the local triad $\mathcal{S}^*$ to coincide with the center of mass of the cross section. Furthermore, the 6×6 stiffness matrix K^* was assumed to be a block diagonal matrix, with null off-diagonal 3×3 blocks, a severe limitation of the range of applicability of the method. Their approach made use of Rodrigues parameters.

Since the placement of the pole P is restricted to coincide with the center of mass, the linear part of (35) need not be satisfied in this case. Furthermore, for Rodrigues parameters the expression of the strain change within the step (40) and (41) can be also written as

$$\underline{\hat{e}}_f^* - \underline{\hat{e}}_i^* = \left(\frac{\alpha_f + \alpha_i}{2}\right)^T \Delta t \left(\underline{\hat{v}}'_m - \widetilde{\breve{v}}_m(\underline{u}'_0 + \underline{u}'_m)\right), \tag{49}$$

$$\underline{\breve{e}}_f^* - \underline{\breve{e}}_i^* = \det\left[\frac{\alpha_f + \alpha_i}{2}\right]\left(\frac{\alpha_f + \alpha_i}{2}\right)^{-1} \Delta t\, \underline{\breve{v}}'_m, \tag{50}$$

while the operator A_m^e is

$$A_m^e = \begin{bmatrix} \dfrac{\alpha_f + \alpha_i}{2} & 0 \\ 0 & \det\left[\dfrac{\alpha_f + \alpha_i}{2}\right]\left(\dfrac{\alpha_f + \alpha_i}{2}\right)^{-T} \end{bmatrix}. \tag{51}$$

These expressions can be readily compared with the ones given in [7].

5.2 *Scheme 2*

Scheme 2 was introduced by Bauchau [19, 18] within the framework of a Galerkin approximation of the equations of motion written in the symmetric hyperbolic form. Here, they are cast as finite difference approximations characterized by the following choice of operators

$$A_m = \left(\frac{A_f + A_i}{2}\right)^{-T}, \quad A_m^{v_f} = A_m^{v_i} = \epsilon \frac{A_f + A_i}{2}, \tag{52}$$

where ϵ is given by (12). This choice satisfies the angular part of condition (35) for the same reasons as those developed for *scheme 1.* For the linear part, we have

$$\alpha_f^T \left(\frac{\alpha_f+\alpha_i}{2}\right)^{-T} + \frac{\Delta t}{2}\,\epsilon \left(\frac{\alpha_f+\alpha_i}{2}\right)^{T} \widetilde{\breve{v}}_m \left(\frac{\alpha_f+\alpha_i}{2}\right)^{-T}$$
$$= \left(\frac{R^{*T}+I}{2}\right)^{-1} \left(I - \frac{\epsilon}{4}\,\widetilde{p}^*\,R^{*T} - \frac{\epsilon}{4}\,\widetilde{p}^*\right)$$
$$= \left(\frac{R^{*T}+I}{2}\right)^{-1} \left(\frac{R^{*T}+I}{2}\right) = I, \tag{53}$$

where property (11) was used again. Similar developments show that condition (36) is satisfied as well.

6 Energy preserving schemes derived from the fixed pole equations

We now examine schemes that are based on discretizations of the fixed pole eqs. (26). The following discretization of these equations is proposed

$$\frac{C_f^{-T} M^* \underline{v}_f^* - C_i^{-T} M^* \underline{v}_i^*}{\Delta t} - \left(C_m^{e-T} K^* \underline{e}_m^*\right)' = \underline{q}_{m(O)}, \tag{54}$$

with an average fixed pole velocity given by

$$\underline{v}_{m(O)} = C_m\,\underline{v}_m^*. \tag{55}$$

C_m and C_m^e are yet unknown, suitable approximations of C. Proceeding as for the moving pole discretization, the work done by the discretized inertial forces is evaluated first by multiplying eq. (54) by $\Delta t\ \underline{v}_m^T$ and integrating over the length of the beam to find

$$\mathcal{W}^I = \int_0^L \underline{v}_{m(O)}^T \left(C_f^{-T} M^* \underline{v}_f^* - C_i^{-T} M^* \underline{v}_i^*\right)\,\mathrm{d}x_1 =$$
$$\int_0^L \underline{v}_m^{*T} \left(C_m^T C_f^{-T} M^* \underline{v}_f^* - C_m^T C_i^{-T} M^* \underline{v}_i^*\right)\,\mathrm{d}x_1. \tag{56}$$

If C_m satisfies the following conditions

$$\left(C_m^T C_f^{-T}\right)^T \underline{v}_m^* = \underline{v}_m^*, \tag{57}$$
$$\left(C_m^T C_i^{-T}\right)^T \underline{v}_m^* = \underline{v}_m^*, \tag{58}$$

and if the average velocity $\underline{v}_m^*$ is selected as the mid-point approximation eq. (37), discretization (54) then implies

$$\mathcal{W}^I = \int_0^L \frac{1}{2}(\underline{v}_f^* + \underline{v}_i^*)^T M^* (\underline{v}_f^* - \underline{v}_i^*)\,\mathrm{d}x_1 = (\mathcal{K}_f - \mathcal{K}_i). \tag{59}$$

6.1 *Scheme 3*

Scheme 3 was proposed by Bottasso and Borri [11], and then again in a more general setting in [12]. The initial and final configurations are related through the following update formulas

$$\underline{u}_f = \underline{u}_i + \Delta t\, \alpha_i H^*[\underline{p}^*]\hat{\underline{v}}^*_m, \tag{60}$$

$$\alpha_f = \alpha_i\, R^*[\underline{p}^*], \quad \underline{p}^* = \Delta t\, \check{\underline{v}}^*_m, \tag{61}$$

where C_m is defined as

$$C_m = \frac{C_f + C_i}{2}. \tag{62}$$

The verification of the angular part of condition (57) is again based on the eigenvector property of rotations, together with the parallelism of $\underline{p}^*$ with the average angular velocity $\check{\underline{v}}^*_m$, $R^*\check{\underline{v}}^*_m = \check{\underline{v}}^*_m$. For the linear part, it is clear that

$$\begin{aligned}\alpha_i^T\alpha_f\,\hat{\underline{v}}^*_m + \alpha_i(\widetilde{u}_f - \widetilde{u}_i)\alpha_f\check{\underline{v}}^*_m &= R^*\hat{\underline{v}}^*_m + (\widetilde{\alpha_i^T(\underline{u}_f - \underline{u}_i)})\,\check{\underline{v}}^*_m \\ &= (R^* - \widetilde{p}^*H^*)\,\hat{\underline{v}}^*_m \\ &= \hat{\underline{v}}^*_m,\end{aligned} \tag{63}$$

where the update eq. (60) and property (10) of rotations have been used.

This way of presenting the scheme allows direct comparison with *schemes 1* and *2*. However, this hides some fundamental characteristics of the configuration tensor. In particular, it can be shown that the configuration tensors C_f and C_i are related by an expression of the following form

$$C_f = D[\underline{\nu}]\, C_i, \tag{64}$$

where $\underline{\nu} = \Delta t\, \underline{v}_m$ are generic translation-rotation parameters, and D possesses the unit eigenvalue, *i.e.*

$$D[\underline{\nu}]\,\underline{\nu} = \underline{\nu}, \tag{65}$$

which generalizes the analogous property of rotations $R[\underline{p}]\,\underline{p} = \underline{p}$. Eq. (65) then ensures that conditions (57) and (58) are verified. Details on the properties of configurations can be found in [12], where the natural (exponential) parameterization is completely developed.

The update equations (60) and (61) imply the following relationship between the spatial derivative of the average velocities $\underline{v}_{m(O)}$ and the strain increments

$$\Delta t\,\underline{v}'_{m(O)} = \begin{bmatrix} H^{-T}\alpha_i & H^{-T}(\widetilde{u}_i - RLH^{-T})\alpha_i) \\ 0 & H^{-T}\alpha_i \end{bmatrix} (\underline{e}^*_f - \underline{e}^*_i), \tag{66}$$

where the operator L satisfies

$$\mathrm{d}H[\underline{p}]\;\underline{v}_{(O)} = L[\underline{p}, \underline{v}_{(O)}]\;\mathrm{d}\underline{p}. \tag{67}$$

Next, the work done by the elastic forces is evaluated by multiplying eq. (54) by $\Delta t\;\underline{v}^T_{m(O)}$ and integrating over the beam span to find

$$\frac{\mathcal{W}^e}{\Delta t} = \int_0^L \underline{v}^T_{m(O)}\left(C_m^{e-T}K^*\underline{e}^*_m\right)'\,\mathrm{d}x_1 = -\int_0^L \underline{v}'^T_{m(O)}C_m^{e-T}K^*\underline{e}^*_m\,\mathrm{d}x_1. \tag{68}$$

Here again, the boundary terms $\underline{v}'^T_{m(O)} C^{e-T}_m K^* \underline{e}^*_m|^L_0$ resulting from the integration by parts vanish. Eqs. (66) are introduced , and C^e_m is selected as

$$C^e_m = \begin{bmatrix} H^{-T}\alpha_i & H^{-T}(\widetilde{u}_i - RLH^{-T})\alpha_i) \\ 0 & H^{-T}\alpha_i \end{bmatrix}. \tag{69}$$

If the average strain is computed using the mid-point rule eq. (43), the work done by the elastic forces becomes

$$\mathcal{W}^e = \int_0^L \frac{1}{2}(\underline{e}^*_f + \underline{e}^*_i)^T K^* (\underline{e}^*_f - \underline{e}^*_i)\, \mathrm{d}x_1 = \mathcal{V}_f - \mathcal{V}_i. \tag{70}$$

Eqs. (59) and (70) then imply the conservation of the total mechanical energy, eq. (45).

7 Discussion

The three schemes presented in the last two sections are all second order accurate, mid-point discretizations of the equations of motion for beams written with respect to a moving or fixed pole. All three discretizations imply the discrete energy preservation statement eq. (45) and are, therefore, unconditionally stable schemes for nonlinear problems. The schemes have been formulated in terms of generic rotation parameters, and can thus be used with any valid parameterization of finite rotations. It should be noted that the above developments readily apply to rigid bodies, which only involve the inertial terms of the equations of motion. Therefore, the energy preserving schemes derived here for beams can be readily used for rigid body dynamics.

It is interesting to note that the conditions that must be met to ensure preservation of energy require the average, body fixed velocity to be the eigenvector corresponding to the unit eigenvalue of discrete operators, see conditions (35, 36) and (57, 58) for the moving and fixed pole formulations, respectively. These conditions can be interpreted as a generalization of the well known eigenvector property of rotations, $R[\underline{p}]\ \underline{p} = \underline{p}$.

As discussed in section 4, the equations of motion for a beam imply the conservation of the total fixed pole momenta, eq. (29). Consider first the discretized equations in the fixed pole form, eqs. (54), in the absence of externally applied loads. Integrating over the length of the beam yields

$$\left(\int_0^L \frac{C_f^{-T} M^* \underline{v}^*_f - C_i^{-T} M^* \underline{v}^*_i}{\Delta t}\, \mathrm{d}x_1 \right)^{\cdot} = 0. \tag{71}$$

The boundary terms $C^{e-T}_m K^* \underline{e}^*_m|^L_0$ resulting from the integration by parts of the elastic force expression vanish for reasons explained earlier. It follows that

$$\left(\int_0^L C^{-T} M^* \underline{v}^*\, \mathrm{d}x_1 \right)_f = \left(\int_0^L C^{-T} M^* \underline{v}^*\, \mathrm{d}x_1 \right)_i, \tag{72}$$

i.e. a statement of discrete momentum preservation. On the other hand, the discrete equations in the moving pole form, eqs. (30), do not preserve momentum, in general. However, if *scheme 1* is used in conjunction with Rodrigues parameters, momentum preservation can be

readily proved. In summary, discretizations based on the fixed pole form of the equations of motion automatically inherit discrete momentum preservation, whereas discretizations based on the moving pole form preserve angular momentum only for a specific choice of the finite rotation parameters.

Consider now two distinct points Q and R rigidly attached to frame $\mathcal{S}^*$, and the vector $\vec{r} = (Q - R)$. The distance between these two points remains a constant. The position and velocity vectors of these two points are related by

$$\underline{u}^Q = \underline{u}^R + \alpha\, \underline{r}^*; \quad \underline{\hat{v}}^{*^Q} = \underline{\hat{v}}^{*^R} + \widetilde{\check{v}}^*\, \underline{r}^*. \tag{73}$$

Let point Q be the reference point used in the analysis. The position updates (31) and (60) for the three schemes can then be written as

$$\underline{u}_f^Q = \underline{u}_i^Q + \Delta t\, \alpha_m \underline{\hat{v}}_m^{*^Q}, \tag{74}$$

where $\alpha_m = (\alpha_f + \alpha_i)/2$, $(\alpha_f + \alpha_i)^{-T}/2$, and $\alpha_i H^*[\underline{p}^*]$, for *schemes 1*, *2*, and *3*, respectively. Introducing eq. (73) yields

$$\underline{u}_f^R = \underline{u}_i^R + \Delta t\, \alpha_m \underline{\hat{v}}_m^{*^R} + \underline{i}, \tag{75}$$

where

$$\underline{i} = \alpha_i (I - R^* + \alpha_i^T \alpha_m \widetilde{p}^*)\, \underline{r}^* \tag{76}$$

is the invariance error. Indeed, if $\underline{i} = 0$, the same update formula will apply to points Q and R, *i.e.* to all points of the section.

For *scheme 1*, the invariance error is

$$\underline{i} = \alpha_i \left(I - R^* + \frac{1}{2}\widetilde{p}^* + \frac{1}{2} R^* \widetilde{p}^* \right) \underline{r}^*, \tag{77}$$

and the scheme is not invariant. Using eq. (7) for R, and expanding in Taylor series yields $|\underline{i}| = O(\Delta t^2)$, *i.e.* an error compatible with the order of the scheme. For *scheme 2*, the invariance error is

$$\underline{i} = \alpha_i \left(I - R^* + \left(\frac{I + R^*}{2} \right)^{-T} \widetilde{p}^* \right) \underline{r}^*, \tag{78}$$

and the scheme is again not invariant. The invariance error for *scheme 3*, is

$$\underline{i} = \alpha_i\, (I - R^* + H^* \widetilde{p}^*)\, \underline{r}^* = 0, \tag{79}$$

where property (11) was used. The scheme is invariant, as already anticipated in the discussion of the fixed pole form of the equations of dynamic equilibrium.

8 Energy decaying schemes

Energy preserving schemes ensure nonlinear unconditional stability to the numerical procedures. However, even such a strong property does not eliminate the possibility of numerical difficulties [20]. In fact, the lack of any form of dissipation mechanism in the presence of

unresolved frequencies can hinder the converge process. A way to circumvent the problem is to derive algorithms implying an energy decay inequality. This ensures unconditional stability in the nonlinear regime, and at the same time provides a mechanism for dissipating the energy content relative to the unresolved frequencies. Such algorithms were first proposed in [8, 11]. References [19, 11] offer an interpretation of the method in the framework of finite elements in time. Reference [12] presents it as a 2-stage FSAL Runge-Kutta method, and gives an analysis of the order of the scheme based on Runge-Kutta theory.

All the energy preserving schemes discussed in the previous sections can be used to derive energy decaying algorithms. The details of this procedure can be found in [19, 11, 12] and will not be repeated here. Furthermore, there is not one single way of deriving an energy decaying scheme given an energy preserving one. At least two slightly different procedures have been suggested in the literature, [12] and [19]. The latter was especially designed to exhibit an improved order behavior in certain cases. However, both methods are based on similar arguments. We give an informal description of the simplest of the two [12] in the following, in order to show the basic ideas.

For a specific energy preserving scheme, the discrete equations of motion can be written symbolically as

$$\mathbb{E}_{i-f,\Delta t}[\frac{\underline{v}_f + \underline{v}_i}{2}, \frac{\underline{e}_f + \underline{e}_i}{2}] = 0, \tag{80}$$

where the subscript $(\bullet)_{i-f,\Delta t}$ indicates that a step of size Δt takes place between t_i and t_f. The discrete equations are clearly functions of the system state at t_i and t_f, but also of the mid point velocities and mid point strains, as indicated explicitly with the notation $\mathbb{E}[\bullet, \bullet]$. The corresponding position and orientation updates can be written as

$$\mathbb{U}_{i-f,\Delta t} = \mathbb{U}_{i-f,\Delta t}[\frac{\underline{v}_f + \underline{v}_i}{2}]. \tag{81}$$

where again the notation explicitly highlights the dependence on the mid point velocities.

Consider now an additional state, indicated with the subscript $(\bullet)_j$, corresponding to time $t_i^+ = t_i + \epsilon$, $\epsilon > 0$, $\epsilon \longrightarrow 0$. An energy decaying algorithm is obtained applying the conserving scheme twice, according to the following coupled scheme

$$\mathbb{E}_{i-f,\Delta t}[\frac{\underline{v}_f + \underline{v}_j}{2}, \frac{\underline{e}_f + \underline{e}_j}{2}] = 0, \tag{82}$$

$$\mathbb{E}_{i-j,\Delta t}[\frac{\underline{v}_f - \underline{v}_j}{6}, \frac{\underline{e}_f - \underline{e}_j}{6}] = 0, \tag{83}$$

with updates

$$\mathbb{U}_{i-f,\Delta t} = \mathbb{U}_{i-f,\Delta t}[\frac{\underline{v}_f + \underline{v}_j}{2}], \tag{84}$$

$$\mathbb{U}_{i-j,\Delta t} = \mathbb{U}_{i-j,\Delta t}[\frac{\underline{v}_f - \underline{v}_j}{6}]. \tag{85}$$

The proof of nonlinear stability is obtained as in the conserving case, *i.e.* by computing the work due to the inertial and elastic forces for each equation of motion. A linear combination of the results then yields the discrete energy decay statment; see [19, 11, 12] for more details of the derivation in some of the cases discussed here.

9 Mechanical constraints

Thus far the discussion has focused on the modeling of the elastic components of the system. However, constraints are a distinguishing feature of multi-body systems. Unconditional stability can be achieved for constrained multi-body systems if the work done by the discretized forces of constraint can be shown to vanish exactly, as should occur in the exact solution. This approach was first introduced in [10], then in [19, 13, 14]. The combination of these two features, the energy preservation or decay for the elastic bodies of the system, and the vanishing of the work done by the forces of constraint, leads to unconditional stability for flexible, nonlinear multi-body systems.

A holonomic constraint connecting a point on body k with a corresponding point on body l can be expressed in general in the form

$$\underline{c}\,[\underline{u}_k, \underline{u}_l, \alpha_k, \alpha_l] = 0. \tag{86}$$

The notation highlights the fact that the constraint will in general specify some relation among the positions and/or orientations at the two points on the bodies. Total differential of (86), yields the differential form of the constraints

$$A^T \underline{v} = 0, \tag{87}$$

that effectively limits the admissible velocities. Using the Lagrange multiplier technique, the forces of constraint acting on the bodies are

$$\underline{f}^C = A\underline{\lambda}, \tag{88}$$

where $\underline{\lambda}$ is a vector of Lagrange multipliers. The forces of constraint are discretized as

$$\underline{f}^C_m = A_m \underline{\lambda}_m, \tag{89}$$

where A_m is a suitable approximation of A, yet to be determined. The work done by these forces is now

$$\mathcal{W}^C = \Delta t\, \underline{v}_m^T A_m \underline{\lambda}_m. \tag{90}$$

A_m is determined based on the requirement that

$$A_m^T \underline{v}_m = \frac{\underline{c}_f - \underline{c}_i}{\Delta t}. \tag{91}$$

The existence of A_m satisfying this relationship is guaranteed by the mean value theorem since $A^T\underline{v} = \dot{\underline{c}}$. The configuration at time t_i is assumed to be compatible, $\underline{c}_i = 0$. The constraint

$$\underline{c}_f = 0 \tag{92}$$

is enforced using the Lagrange multiplier (89), and eq. (91) then implies

$$\mathcal{W}^C = 0. \tag{93}$$

Hence, the nonlinear conservation laws are retained for the constrained system.

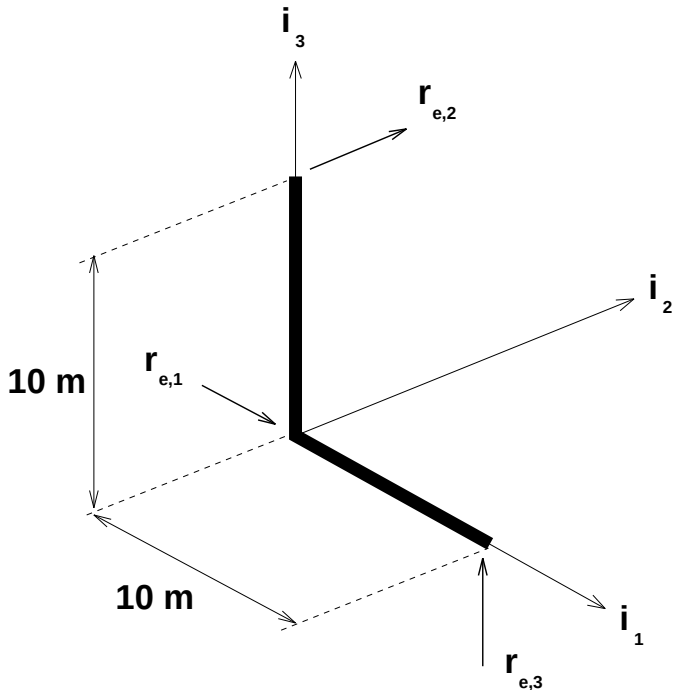

Figure 2: The right angle beam problem.

10 Numerical examples

The predictions of two of the energy preserving schemes discussed in this paper will be presented in this section. Simple, but numerically challenging test problems will be used to compare *schemes 2* and *3*, implemented with Rodrigues parameters and the rotation vector, respectively.

10.1 Right angle beam in free flight

This problem deals with the dynamic response of a beam subjected to loads that induce a complex, three-dimensional tumbling motion. The dynamic response is relatively smooth and the convergence characteristics of *schemes 2* and *3* will be compared. The beam, depicted in fig. 2, is subjected to three forces $\underline{r}_{e,1} = f_0(t)\ \underline{i}_1$, $\underline{r}_{e,2} = f_0(t)\ \underline{i}_2$ and $\underline{r}_{e,3} = f_0(t)\ \underline{i}_3$, with the following time history

$$f_0(t) = \begin{cases} 50t, & 0\ sec\ \leq t < 1\ sec, \\ 100 - 50t, & 1\ sec\ \leq t < 2\ sec, \\ 0, & 2\ sec\ \leq t. \end{cases}$$

The beam has the following physical characteristics: axial stiffness $EA = 0.1\ MN$, shearing stiffness $GK = 0.1\ MN$, bending stiffnesses $EI_{22} = EI_{33} = 100\ N.m^2$, torsional stiffness $GJ = 100\ N.m^2$, mass per unit span $m = 1\ Kg/m$, and mass moment of inertia per unit span $J = 10\ Kg.m$. The spatial discretization consists of ten, two-noded beam elements. Five simulations were conducted with the energy preserving scheme for a total duration

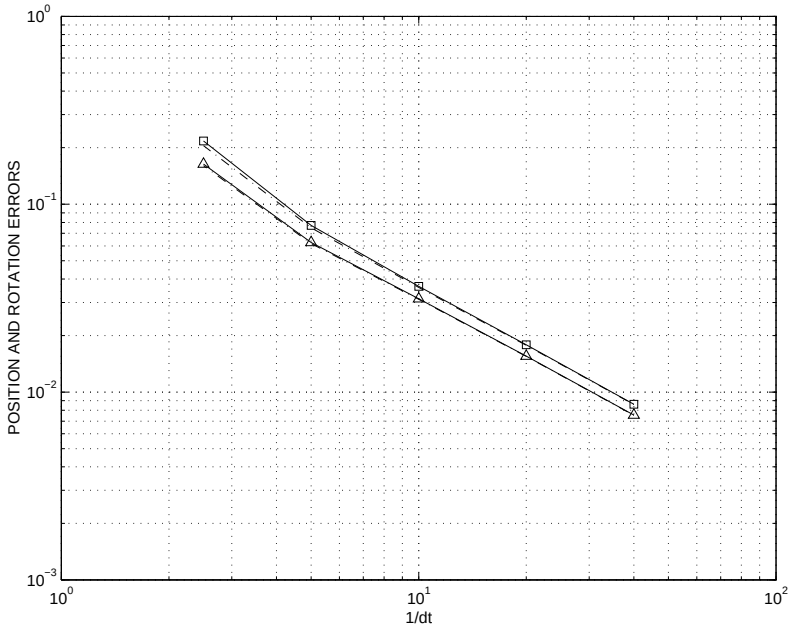

Figure 3: Convergence of position (△) and rotation (□) errors. *Scheme 2*: solid line; *scheme 3*: dash-dotted line.

of 8 *sec*, with time steps $\Delta t = 0.4$, 0.2, 0.1, 0.05, and 0.025 *sec*. Since no analytical solution exists for this problem, a sixth simulation with a time step $\Delta t = 0.003125$ *sec* was performed. This solution was used as a *reference* solution for computing errors of the coarser time discretizations. The results obtained by the two schemes for the reference solution are virtually identical for all the fields.

Results are presented as plots of relative error versus the inverse of the time step size. Relative errors are defined as the norm of the difference of the computed and reference solutions, normalized by the norm of the reference solution. Figs. 3, 4, and 5 show the relative errors in position and rotation, linear and angular velocity, and force and moment, respectively. The predictions of the two schemes are in excellent agreement, and the second order convergence clearly demonstrated for all fields, except the force and moment fields, as expected.

10.2 The four bar mechanism

The second problem deals with the four bar mechanism problem depicted in fig. 6. Bar 1 is of length $L_1 = 0.12$ m and is connected to the ground at point A by means of a revolute joint. Bar 2 is of length $L_2 = 0.24$ m and is connected to bar 1 at point B with a revolute joint. Finally, bar 3 is of length $L_3 = 0.12$ m and is connected to bar 2 and the ground at points C and D, respectively, by means of two revolute joints. In the reference configuration, the bars of this planar mechanism intersect each other at 90 degree angles and the axes of rotation of the revolute joints at points A, B, and D are normal to the plane of the mechanism. However, the axis of rotation of the revolute joint at point C is at a 5 degree

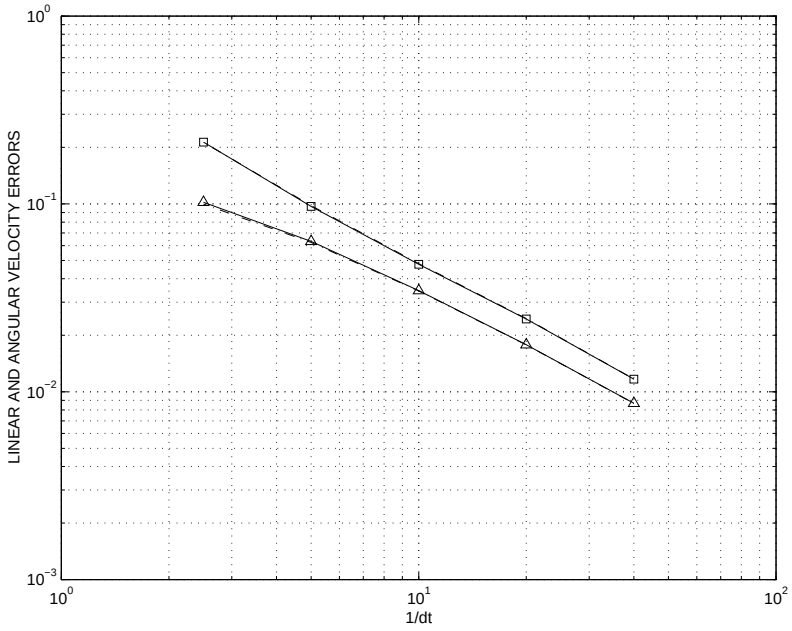

Figure 4: Convergence of linear ($\triangle$) and angular ($\square$) velocity errors. *Scheme 2*: solid line; *scheme 3*: dash-dotted line.

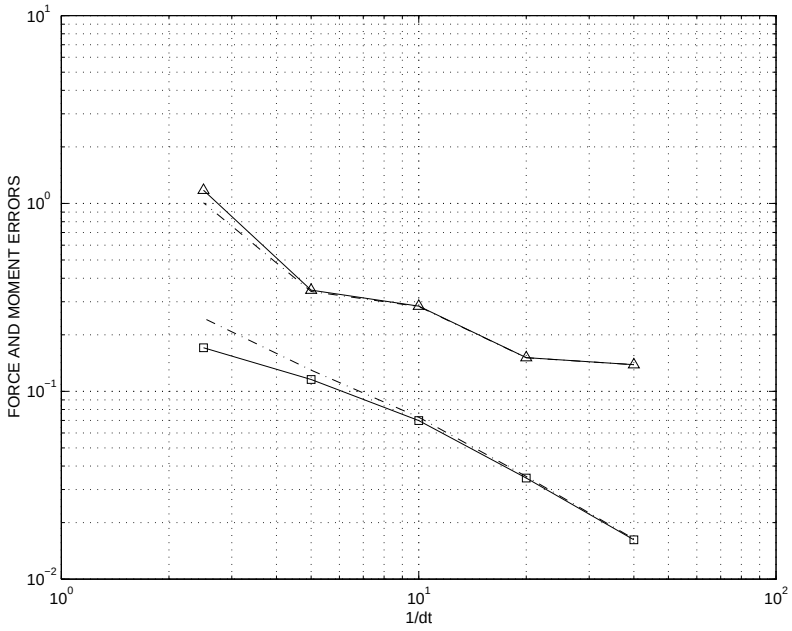

Figure 5: Convergence of force ($\triangle$) and moment ($\square$) errors. *Scheme 2*: solid line; *scheme 3*: dash-dotted line.

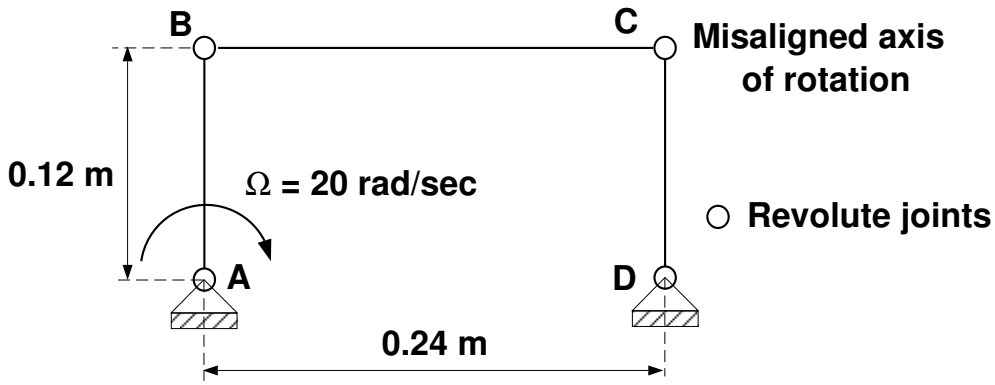

Figure 6: The four bar mechanism problem.

angle with respect to this normal to simulate an initial defect in the mechanism. A torque is applied on bar 1 at point A so as to enforce a constant angular velocity $\Omega = 20\ rad/sec$. If the bars were infinitely rigid, no motion would be possible as the mechanism locks. For elastic bars, motion becomes possible, but generates large, rapidly varying internal forces. Bar 1 has the following physical characteristics: axial stiffness $EA = 40\ MN$, bending stiffnesses $EI_{22} = EI_{33} = 0.24\ MN.m^2$, torsional stiffness $GJ = 0.28\ MN.m^2$, and mass per unit span $m = 3.2\ Kg/m$. Bars 2 and 3 have the following physical characteristics: axial stiffness $EA = 40\ MN$, bending stiffnesses $EI_{22} = EI_{33} = 24\ KN.m^2$, torsional stiffness $GJ = 28\ KN.m^2$, and mass per unit span $m = 1.6\ Kg/m$.

This problem was simulated for a total of 0.5 sec using the energy decaying schemes. If the four revolute joints had their axes of rotation orthogonal to the plane of the mechanism, the response of the system would be purely planar, and bars 1 and 3 would rotate at constant angular velocities around points A and D, respectively. The initial defect in the mechanism causes a markedly different response. Bar 1 rotates at a constant angular velocity under the effect of the applied torque, but bar 3 now oscillates back and forth, never completing an entire turn. When the direction of rotation of bar 3 reverses, bar 2 undergoes large rotations, instead of near translation, and sharp increases in velocities are observed, as depicted in fig. 7. Furthermore, the response is three dimensional as shown in fig. 8 which depicts the time history of out-of-plane displacements at point C. Point C undergoes a 1.5 mm maximum out-of-plane displacement.

The time history of the three components of the internal force at the root of bar 1 are shown in fig. 9, whereas fig. 10 shows the time history of components of twisting and bending moments at the same location. These large internal forces are all caused by the initial imperfection of the mechanism. The two schemes are in very close agreement, and yield smooth time history responses for all quantities.

Next, the prediction of the energy preserving scheme are presented in figs. 11 and 12 that depict the velocities at point C, and the quarter-point forces in bar 1, respectively. These figures should be compared with figs. 7 and 9, respectively, obtained with the energy decaying schemes. Clearly, very high frequency oscillations of a purely numerical origin are present in the predictions of the energy preserving scheme. The high frequency numerical

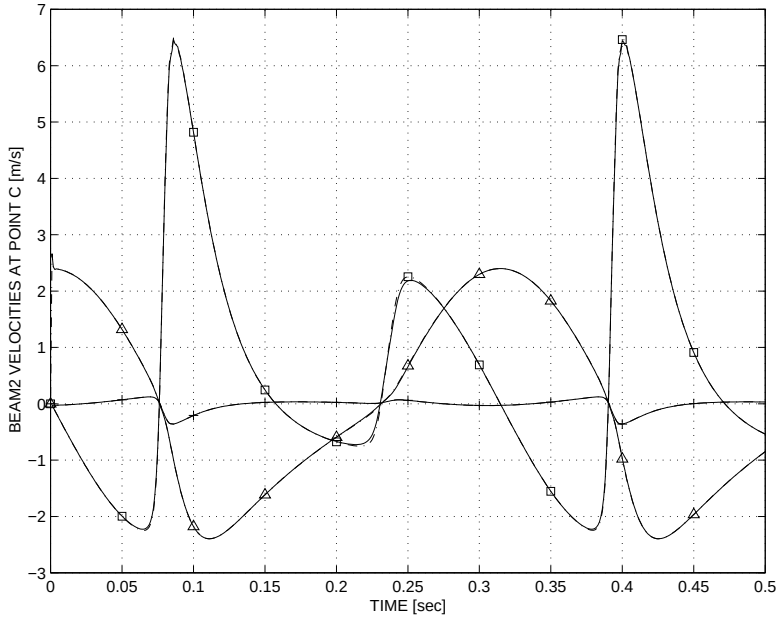

Figure 7: Time history of velocities at point C. Velocity components v_1 ($\triangle$), v_2 ($\square$), and v_3 ($+$). *Scheme 2*: solid line; *scheme 3*: dash-dotted line.

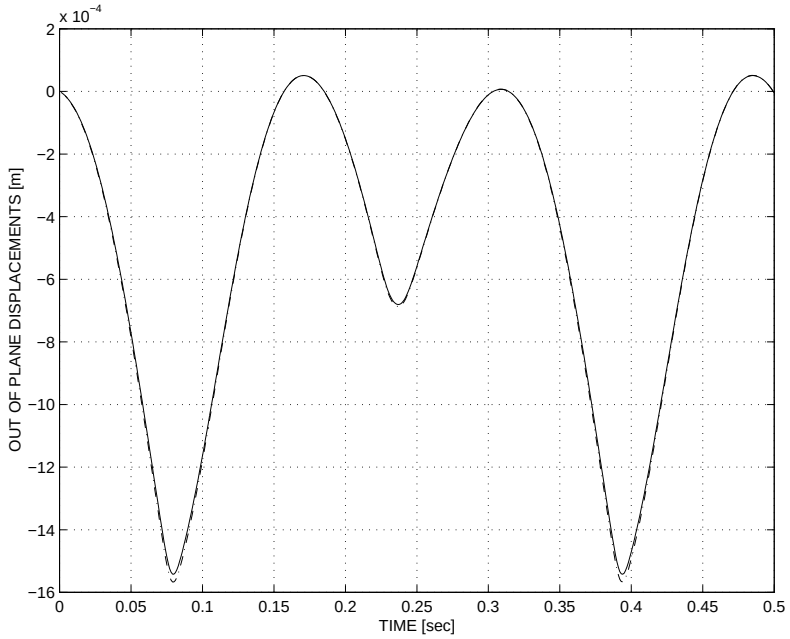

Figure 8: Time history of out-of-plane displacements at point C. *Scheme 2*: solid line; *scheme 3*: dash-dotted line.

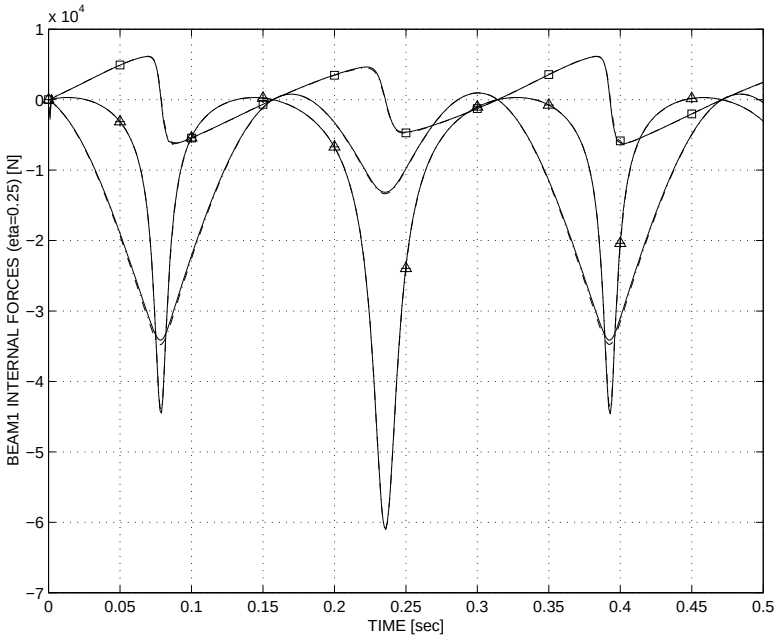

Figure 9: Time history of the quarter-point forces in bar 1, in local axes. Axial ($\triangle$), in-plane shear ($\square$), and out-of-plane shear ($+$) forces. *Scheme 2*: solid line; *scheme 3*: dash-dotted line.

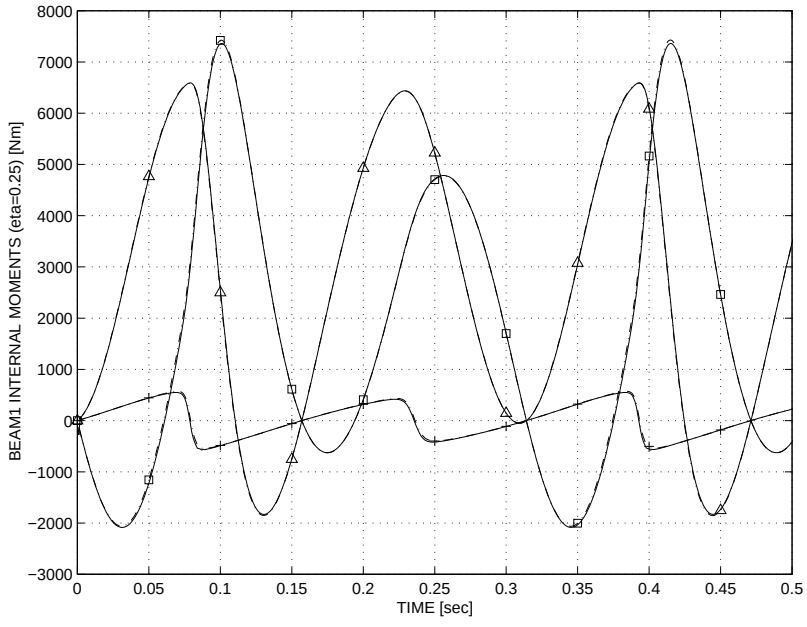

Figure 10: Time history of quarter-point moments in bar 1, in local axes. Torque ($\triangle$), in-plane bending ($\square$), and out-of-plane bending moments ($+$). *Scheme 2*: solid line; *scheme 3*: dash-dotted line.

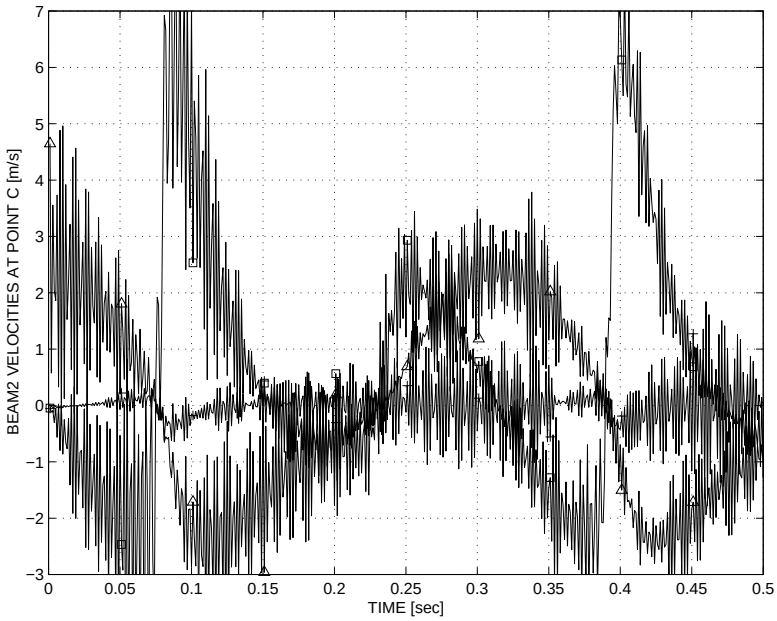

Figure 11: Time history of velocities at point C, using the energy preserving *scheme 2*. Velocity components v_1 ($\triangle$), v_2 ($\square$), and v_3 ($+$).

dissipation featured by the energy decaying schemes completely eliminates this undesirable numerical noise.

10.3 The actuated beam problem

The last problem deals with the actuated beam problem depicted in fig. 13. A cantilevered beam of length $L = 2.4\ m$ with a tip mass $M_T = 25\ Kg$ is actuated at its mid point M by a crank and link mechanism. The crank of length $L_c = 0.20\ m$ is connected to the ground at point A and to a link of length $L_l = 0.20 \times \sqrt{2}\ m$ at point B. The link is connected to the beam at point M. All connections are by means of revolute joints. A torque is applied at point A so as to enforce a constant angular velocity $\Omega = \pi\ rad/sec$. The beam has the following physical properties: axial stiffness $EA = 91.2\ MN$, bending stiffnesses $EI = 14.2\ KN.m^2$, shearing stiffness $GK = 91.2\ MN$, and mass per unit span $m = 2.1\ Kg/m$. The properties of the link are: axial stiffness $EA = 44\ MN$, bending stiffnesses $EI = 0.3\ MN.m^2$, shearing stiffness $GK = 14\ MN$, and mass per unit span $m = 1.6\ Kg/m$. The crank is a rigid body with a mass moment of inertia $I_c = 6\ Kg.m^2$.

The response of the simulation is presented for a complete revolution of the crank. The energy decaying version of the algorithms was used for this example. Fig. 14 shows the tip displacements of the beam. Elastic vibrations are superposed onto the overall motion imparted by the crank. Note the very large transverse deflection of the beam, of up to $0.7\ m$, *i.e.* 30% of its length. The axial and transverse shear forces at the beam quarter-point, and the axial force at the link mid-point are depicted in figs. 15 and 16, respectively. Here again, excellent agreement is observed between the two schemes.

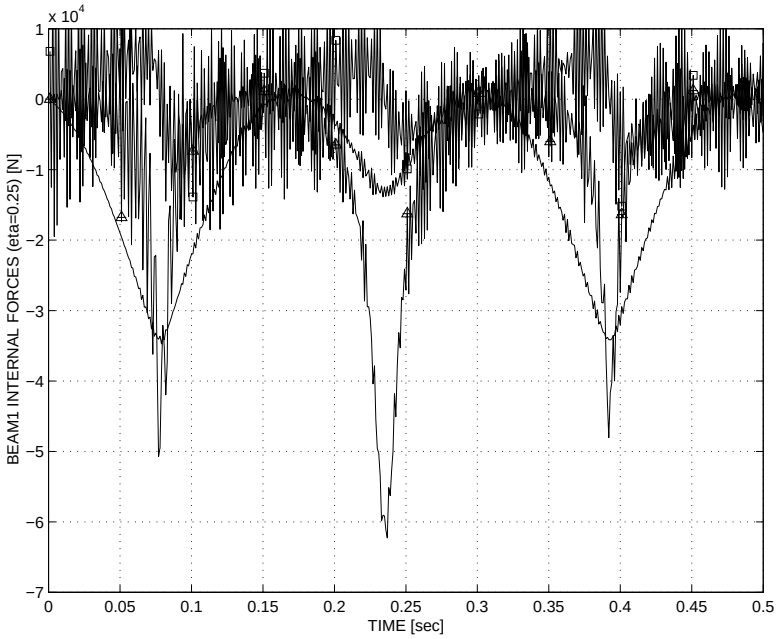

Figure 12: Time history of the quarter-point forces in bar 1, in local axes, using the energy preserving *scheme 2*. Axial (△), in-plane shear (□), and out-of-plane shear (+) forces.

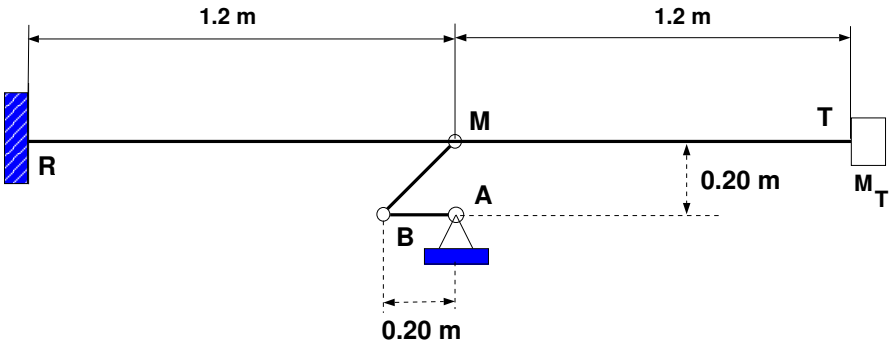

Figure 13: The actuated beam problem.

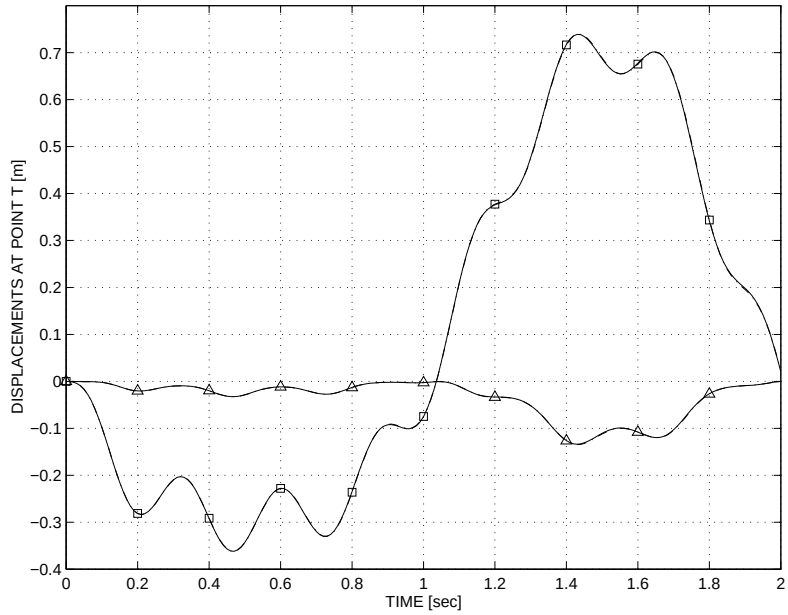

Figure 14: Time history of beam tip displacements. u_1 ($\triangle$); u_2 ($\square$). *Scheme 2*: solid line; *scheme 3*: dash-dotted line.

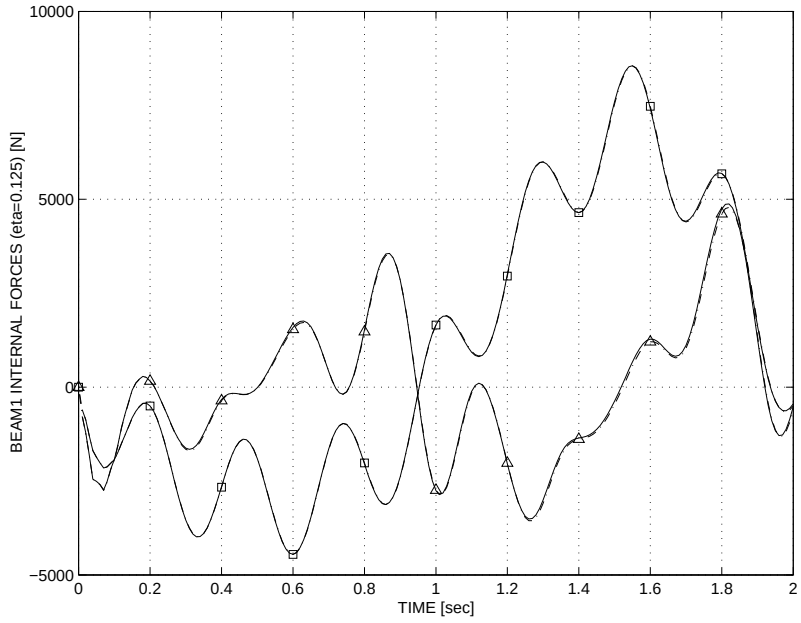

Figure 15: Time history of quarter-point internal forces in the beam, in local axes. Axial force ($\triangle$); shear force ($\square$). *Scheme 2*: solid line; *scheme 3*: dash-dotted line.

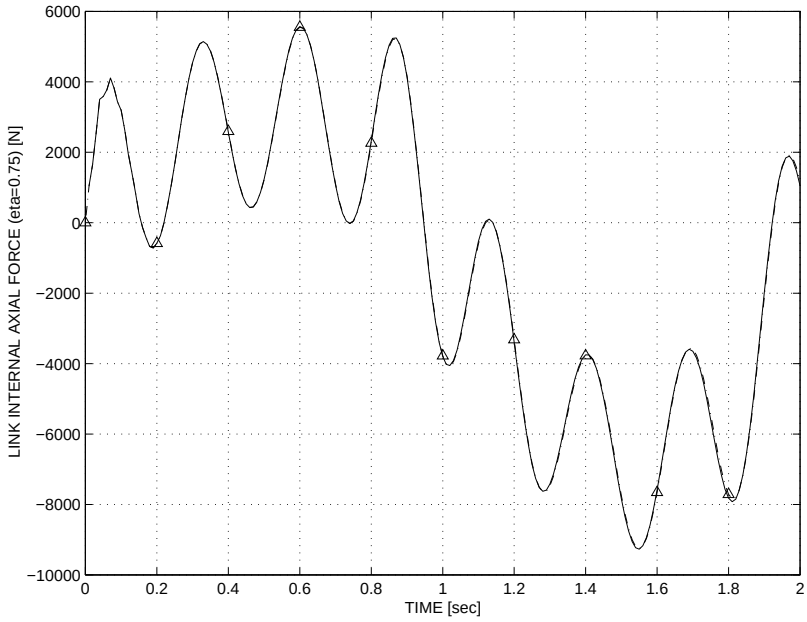

Figure 16: Time history of the link mid-point axial force ($\triangle$). *Scheme 2*: solid line; *scheme 3*: dash-dotted line.

11 Conclusions

Energy preserving schemes achieve unconditional stability for nonlinear systems by establishing discrete energy preservation statements. These schemes have been presented by various authors within drastically different frameworks: finite difference schemes based on a mid-point approximation, Galerkin and time discontinuous Galerkin approximations of the equations of motion written in the symmetric hyperbolic form, finite elements in time, and 2-stage FSAL Runge-Kutta methods. Furthermore, different types of parameterization of finite rotations were used in the various formulations.

This paper has presented a unified, finite difference framework which readily allows comparing the various schemes and their respective properties. In fact, all the schemes reviewed here are second order accurate discretizations of the governing equations of motion, and hence, *are all equivalent within a second order approximation.* Schemes based on the fixed pole form of the equations of motion also inherit a discrete preservation statement of total fixed pole momentum, whereas one scheme based on the moving pole formulation presents this additional feature for a specific choice of the rotation parameters only. Furthermore, invariance on the choice of the reference line is guaranteed by the fixed pole schemes.

Numerical examples have shown that the predictions of two of these schemes are in very close agreement with each other, as expected. The need for the high frequency numerical dissipation provided by energy decaying schemes was also demonstrated.

References

[1] T.J.R. Hughes. *The Finite Element Method*. Prentice Hall, Inc., Englewood Cliffs, New Jersey, 1992.

[2] N.M. Newmark. A method of computation for structural dynamics. *Journal of the Engineering Mechanics Division*, 85:67–94, 1959.

[3] A. Cardona and M. Géradin. Time integration of the equations of motion in mechanism analysis. *Computers and Structures*, 33(3):801–820, 1989.

[4] H.M. Hilber, T.J.R. Hughes, and R.L. Taylor. Improved numerical dissipation for time integration algorithms in structural dynamics. *Earthquake Engineering and Structural Dynamics*, 5:282–292, 1977.

[5] J.C. Simo and K. Wong. Unconditionally stable algorithms for rigid body dynamics that exactly preserve energy and momentum. *International Journal for Numerical Methods in Engineering*, 31:19–52, 1991.

[6] J.C. Simo and N. Tarnow. The discrete energy-momentum method. Conserving algorithms for nonlinear dynamics. *ZAMP*, 43:757–792, 1992.

[7] J.C. Simo, N. Tarnow, and M. Doblare. Non-linear dynamics of three-dimensional rods: Exact energy and momentum conserving algorithms. *International Journal for Numerical Methods in Engineering*, 38:1431–1473, 1995.

[8] O.A. Bauchau and N.J. Theron. Energy decaying scheme for non-linear beam models. *Computer Methods in Applied Mechanics and Engineering*, 134:37–56, 1996.

[9] O.A. Bauchau and T. Joo. Computational schemes for nonlinear elasto-dynamics. *International Journal for Numerical Methods in Engineering*, 45:693–719, 1999.

[10] O.A. Bauchau and N.J. Theron. Energy decaying schemes for nonlinear elastic multibody systems. *Computers and Structures*, 59:317–331, 1996.

[11] C.L. Bottasso and M. Borri. Energy preserving/decaying schemes for non-linear beam dynamics using the helicoidal approximation. *Computer Methods in Applied Mechanics and Engineering*, 143:393–415, 1997.

[12] C.L. Bottasso and M. Borri. Integrating finite rotations. *Computer Methods in Applied Mechanics and Engineering*, 164:307–331, 1998.

[13] C.L. Bottasso, M. Borri, and L. Trainelli. Integration of elastic multibody systems by invariant conserving/dissipating algorithms. Part I: formulation. *Computer Methods in Applied Mechanics and Engineering*, 190:3669–3699, 2001.

[14] C.L. Bottasso, M. Borri, and L. Trainelli. Integration of elastic multibody systems by invariant conserving/dissipating algorithms. Part II: numerical schemes and applications. *Computer Methods in Applied Mechanics and Engineering*, 190:3701–3733, 2001.

[15] T.R. Kane. *Dynamics*. Holt, Rinehart and Winston, Inc, New York, 1968.

[16] E.J. Haug. *Intermediate Dynamics*. Prentice Hall, Inc., Englewood Cliffs, New Jersey, 1992.

[17] A. Cardona. *An Integrated Approach to Mechanism Analysis*. PhD thesis, Université de Liège, 1989.

[18] O.A. Bauchau and D.H. Hodges. Analysis of nonlinear multi-body systems with elastic couplings. *Multibody System Dynamics*, 3:168–188, 1999.

[19] O.A. Bauchau. Computational schemes for flexible, nonlinear multi-body systems. *Multibody System Dynamics*, 2:169–225, 1998.

[20] O.A. Bauchau, G. Damilano, and N.J. Theron. Numerical integration of nonlinear elastic multi-body systems. *International Journal for Numerical Methods in Engineering*, 38:2727–2751, 1995.